

1 A channel selection method for hyperspectral  
2 atmospheric infrared sounders based on  
3 layering

4 Shujie Chang<sup>1,2,3</sup>, Zheng Sheng<sup>1,2</sup>, Huadong Du<sup>1,2</sup>, Wei Ge<sup>1,2</sup> and  
5 Wei Zhang<sup>1,2</sup>

6 <sup>1</sup> College of Meteorology and Oceanography, National University of  
7 Defense Technology, Nanjing, China

8 <sup>2</sup> Collaborative Innovation Center on Forecast and Evaluation of  
9 Meteorological Disasters, Nanjing University of Information  
10 Science and Technology, Nanjing, China

11 <sup>3</sup> South China Sea Institute for Marine Meteorology, Guangdong  
12 Ocean University, Zhanjiang, China

13

14 **Correspondence:** Zheng Sheng (19994035@sina.com)

15

16 **Abstract.** This study introduces an effective channel selection  
17 method for hyperspectral infrared sounders. The method is  
18 illustrated for the Atmospheric InfraRed Sounder (AIRS) instrument.  
19 The results are as follows: (1) Using the improved channel selection  
20 (ICS), the atmospheric retrievable index is more stable, the value  
21 reaching 0.54. The coverage of the weighting functions is more  
22 evenly distributed over height with this method; (2) Statistical

23 inversion comparison experiments show that the accuracy of the  
24 retrieval temperature, using the improved channel selection method  
25 in this paper, is consistent with that of 1Dvar channel selection. In  
26 the stratosphere and mesosphere especially, from 10 hPa to 0.02 hPa,  
27 the accuracy of the retrieval temperature of our improved channel  
28 selection method is improved by about 1 K. Also at lower heights,  
29 the accuracy of the retrieval temperature of ICS is improved; (3)  
30 Statistical inversion comparison experiments for four different  
31 regions illustrate latitudinal and seasonal variations and better  
32 performance of ICS compared to the NWP Channel Selection (NCS)  
33 and Primary Channel Selection (PCS) methods. The ICS method  
34 shows potential for future applications.

35

## 36 **1 Introduction**

37 Since the successful launch of the first meteorological satellite,  
38 TIROS in the 1960s, satellite observation technology has developed  
39 rapidly. Meteorological satellites observe the Earth's atmosphere  
40 from space and are able to record data from regions which are  
41 otherwise difficult to observe. Satellite data greatly enrich the  
42 content and range of meteorological observations, and consequently,  
43 atmospheric exploration technology and meteorological observations  
44 have taken us to a new stage in our understanding of weather

45 systems and related phenomena (Fang, 2014). From the perspective  
46 of vertical atmospheric observation, satellite instruments are  
47 developing rapidly. In their infancy, the traditional infrared  
48 measurement instruments for detecting atmospheric temperature and  
49 moisture profiles, such as TOVS (Smith et al., 1991) or HIRS in  
50 ATOVS (Chahine, 1972; Li et al., 2000; Liu, 2007), usually  
51 employed filter spectrometry. Even though such instruments have  
52 played an important role in improving weather prediction, it is  
53 difficult to continue to build upon improvements in terms of  
54 observation accuracy and vertical resolution due to the limitation of  
55 low spectral resolution. By using this kind of filter-based  
56 spectroscopic measurement instrument, therefore, it is difficult to  
57 meet today's needs in numerical weather prediction (Eyre et al.,  
58 1993; Prunet et al., 2010; Menzel et al., 2018). To meet this  
59 challenge, a series of plans for the creation of high-spectral  
60 resolution atmospheric measurement instruments has been executed  
61 in the United States and in Europe in recent years: One example is  
62 the AIRS (Atmospheric InfraRed Sounder) on the Earth Observation  
63 System, "Aqua", launched on May 4, 2002 from the United States.  
64 AIRS has 2378 spectral channels providing sensitivity from the  
65 ground to up to about 65 km of altitude (Aumann et al., 2003;  
66 Hoffmann and Alexander, 2009; Gong et al., 2011). The United

67 States and Europe, in 2010 and in 2007, also installed the CRIS  
68 (Cross-track Infrared Sounder) and the IASI (Infrared Atmospheric  
69 Sounding Interferometer) on polar-orbiting satellites.

70 China also devotes great importance to the development of such  
71 advanced sounding technologies. In the early 1990s, the National  
72 Satellite Meteorological Center began to investigate the principles  
73 and techniques of hyperspectral resolution atmospheric observations.  
74 China's development of interferometric atmospheric vertical  
75 detectors eventually led to the launch of Fengyun No. 3, on May 27,  
76 2008, and Fengyun No. 4 on December 11, 2016, both of which  
77 were equipped with infrared atmospheric instruments. How best to  
78 use the hyperspectral resolution observation data obtained from  
79 these instruments, to obtain reliable atmospheric temperature and  
80 humidity profiles, is an active area of study in atmospheric inversion  
81 theory.

82 Due to technical limitations, only a limited number of channels  
83 could at first be built into the typical satellite instruments. In this  
84 case, channel selection generally involved controlling the channel  
85 weighting function by utilizing the spectral response characteristics  
86 of the channel (such as center frequency and bandwidth). With the  
87 development of measurement technology, increasing numbers of  
88 hyperspectral detectors were carried on meteorological satellites.

89 Due to the large number of channels and data supported by such  
90 instruments today (such as AIRS with 2378 channels and IASI with  
91 8461 channels), it has proven extremely cumbersome to store,  
92 transmit, and process such data. Moreover, there is often a close  
93 correlation between the channel, causing an ill-posedness of the  
94 inversion, potentially compromising accuracy of the retrieval  
95 product based on hyperspectral resolution data.

96 However, hyperspectral detectors have many channels and  
97 provide real-time mode prediction systems with vast quantities of  
98 data, which can significantly improve prediction accuracy. But, if all  
99 the channels are used to retrieve data, the retrieval time considerably  
100 increases. Even more problematic are the glut of information  
101 produced, and the unsuitability of the calculations for real-time  
102 forecasting. Concurrently, the computer processing power must be  
103 large enough to meet the demands of simulating all the channels  
104 simultaneously within the forecast time. In order to improve the  
105 calculation efficiency and retrieval quality, it is very important to  
106 properly select a set of channels that can provide as much  
107 information as possible.

108 Many researchers have studied channel selection algorithms. Menke  
109 (1984) first chose channels using a data precision matrix method.  
110 Aires et al. (1999) made the selection using the Jacobian matrix,

111 which has been widely used since then (Aires et al., 2002; Rabier et  
112 al., 2010). Rodgers (2000) indicated that there are two useful  
113 quantities in measuring the information provided by the observation  
114 data: Shannon information content and degrees of freedom. The  
115 concept of information capacity then became widely used in satellite  
116 channel selection. In 2007, Xu (2007) compared the Shannon  
117 information content with the relative entropy, analyzing the  
118 information loss and information redundancy. In 2008, Du et al.  
119 (2008) introduced the concept of the atmospheric retrievable index  
120 (ARI) as a criterion for channel selection, and in 2010, Wakita et al.  
121 (2010) produced a scheme for calculating the information content of  
122 the various atmospheric parameters in remote sensing using  
123 Bayesian estimation theory. Kuai et al. (2010) analyzed both the  
124 Shannon information content and degrees of freedom in channel  
125 selection when retrieving CO<sub>2</sub> concentrations using thermal infrared  
126 remote sensing and indicated that 40 channels could contain 75% of  
127 the information from the total channels. Cyril et al. (2003) proposed  
128 the optimal sensitivity profile method based on the sensitivity of  
129 different atmospheric components. Lupu et al. (2012) used degrees  
130 of freedom for signals (DFS) to estimate the amount of information  
131 contained in observations in the context of observing system  
132 experiments. In addition, the singular value decomposition method

133 has also been widely used for channel selection (Prunet et al., 2010;  
134 Zhang et al., 2011; Wang et al., 2014). In 2017, Chang et al. (2017)  
135 selected a new set of Infrared Atmospheric Sounding Interferometer  
136 (IASI) channels using the channel score index (CSI). Richardson et  
137 al. (2018) selected 75 from 853 channels based on the high  
138 spectral-resolution oxygen A-band instrument on NASA's Orbiting  
139 Carbon Observatory-2 (OCO-2), using information content analysis  
140 to retrieve the cloud optical depth, cloud properties, and position.

141 Today's main methods for channel selection use only the  
142 weighting function to study appropriate numerical methods, such as  
143 the data precision matrix method (Menke, 1984), singular value  
144 decomposition method (Prunet et al., 2010; Zhang et al., 2011; Wang  
145 et al., 2014), and the Jacobi method (Aires et al., 1999; Rabier et al.,  
146 2010). The use of the methods allows sensitive channels to be  
147 selected. The above-mentioned studies also take into account the  
148 sensitivity of each channel to atmospheric parameters during channel  
149 selection, while ignoring some factors that impact retrieval results.  
150 The accuracy of retrieval results depends not only on the channel  
151 weighting function but also on the channel noise, background field,  
152 and the retrieval algorithm.

153 Channel selection mostly uses the information content and delivers the  
154 largest amount of information for the selected channel combination

155 during the retrieval (Rodgers, 1996; Du et al., 2008; He et al., 2012;  
156 Richardson et al., 2018).

157 This method has made great breakthroughs in both theory and  
158 practice, and the concept of information content itself does consider  
159 all the height dependencies of the kernel matrix  $K$  (Rodgers, 2000).  
160 However, earlier works have neglected the height dependencies of  $K$   
161 for simplicity. This paper uses the atmospheric retrievable index  
162 (ARI) as the index, which is based on information content (Du et al.,  
163 2008; Richardson et al. 2018). Channel selection is made at different  
164 heights, and an effective channel selection scheme is proposed  
165 which fully considers various factors, including the influence of  
166 different channels on the retrieval results at different heights. This  
167 ensures the best accuracy of the retrieval product when using the  
168 selected channel. In addition, statistical inversion comparison  
169 experiments are used to verify the effectiveness of the method.

170

## 171 **2 Channel selection indicator, scheme and method**

### 172 **2.1 Channel selection indicator**

173 According to the concept of information content, the information  
174 content contained in a selected channel of a hyperspectral instrument  
175 can be described as  $H$  (Rodgers, 1996; Rabier et al., 2010). The final  
176 expression of  $H$  is:



177

$$H = -\frac{1}{2} \ln |\hat{S} S_a^{-1}|$$

178

$$= -\frac{1}{2} \ln |(S_a - S_a K^T (K S_a K^T + S_\varepsilon)^{-1} K S_a) S_a^{-1}|, \quad (1)$$

180

181 where  $S_a$  is the error covariance matrix of the background or the  
182 estimated value of atmospheric profile,  $S_\varepsilon$  represents the  
183 observation error covariance matrix of each hyperspectral detector  
184 channel,  $\hat{S} = (S_a - S_a K^T (K S_a K^T + S_\varepsilon)^{-1} K S_a)$  denotes the  
185 covariance matrix after retrieval,  $K$  is the weighting function matrix.

186 In order to describe the accuracy of the retrieval results visually  
187 and quantitatively, the atmospheric retrievable index (ARI),  $p$ , (Du et  
188 al., 2008) is defined as follows:

189

$$p = 1 - \exp\left(\frac{1}{2n} \ln |\hat{S} S_a^{-1}|\right), \quad (2)$$

191

192 Assuming that before and after the retrieval, the ratio of the root  
193 mean square error of each element in the atmospheric state vector is  
194  $1-p$ , then  $|\hat{S} S_a^{-1}| = (1-p)^{2n}$  is derived. By inverting the equation,  
195 the ARI that is  $p$  can be obtained in Eq. (2), which indicates the  
196 relative portion of the error that is eliminated by retrieval. In fact,  
197 before and after retrieval, the ratio of the root mean square error of

198 each element cannot be  $1-p$ . Therefore,  $p$  defined by Eq. (1) is  
199 actually an overall evaluation of the retrieval result.

200

## 201 **2.2 Channel selection scheme**

202 The principle of channel selection is to find the optimum channel  
203 combination after numbering the channels. This combination makes  
204 the information content,  $H$ , or the ARI defined in this paper as large  
205 as possible, in order to maintain the highest possible accuracy in the  
206 retrieval results.

207 Let there be  $M$  layers in the vertical direction of the atmosphere  
208 and  $N$  satellite channels. Selecting  $n$  from  $N$  channels, there will be  
209  $C_N^n$  combinations in each layer, leading  $C_N^n$  calculations to get  $C_N^n$   
210 kinds of  $p$  results. Furthermore, there are  $M$  layers in the vertical  
211 direction of the atmosphere. Therefore, the entire atmosphere must  
212 be calculated  $M \cdot C_N^n$  times. However, the calculation  $M \cdot C_N^n$  times  
213 will be particularly large, which makes this approach impractical in  
214 calculating  $p$  for all possible combinations. Therefore, it is necessary  
215 to design an effective calculation scheme, and such a scheme, i.e., a  
216 channel selection method, using iteration is proposed, called the  
217 “sequential absorption method” (Dudhia et al., 2002; Du et al., 2008).  
218 The method’s main function is to select (“absorb”) channels one by  
219 one, taking the channel with the maximum value of  $p$ . Through  $n$

220 iterations, n channels can be selected as the final channel

221 combination. The steps are as follows:

222 (I) The expression of information content in a single channel:

223 First, we use only one channel for retrieval. A row vector,  $k$ , in the  
 224 weighting function matrix,  $K$ , is a weighting function corresponding  
 225 to the channel. After observation in this channel, the error covariance  
 226 matrix is:

$$227 \hat{S} = S_a - S_a k^T (s_\varepsilon + k S_a k^T)^{-1} k S_a. \quad (3)$$

228 It should be noted that  $(s_\varepsilon + k S_a k^T)$  is a scalar value in Eq. (3),

229 so Eq. (3) can be converted to:

$$230 \hat{S} = \left( I - \frac{S_a k^T k}{(s_\varepsilon + k S_a k^T)} \right) S_a = \left( I - \frac{(k S_a)^T k}{(s_\varepsilon + k (k S_a)^T)} \right) S_a. \quad (4)$$

231 Substituting Eq. (4) into Eq. (2) gives:

$$232 p = 1 - \exp\left(\frac{1}{2n} \ln\left(\left| I - \frac{(k S_a)^T k}{(s_\varepsilon + k (k S_a)^T)} \right|\right)\right). \quad (5)$$

233

234 (II) Simplification of Eq. (5) for calculating the p value:

235 Since  $S_a$  and  $S_\varepsilon$  are positive definite symmetric matrices, they

236 can be decomposed into  $S_a = (S_a^{1/2})^T (S_a^{1/2})$  and

$$237 S_\varepsilon = (S_\varepsilon^{1/2})^T (S_\varepsilon^{1/2}).$$

238

$$239 \text{ Define } R = S_\varepsilon^{1/2} K S_a^{1/2}. \quad (6)$$

240

241 The matrix R can then be regarded as a weighting function matrix,  
 242 normalized by the observed error and a priori uncertainty. A row  
 243 vector of R,  $r = S_\varepsilon^{-1/2} k S_a^{1/2}$ , represents the normalized weighting  
 244 function matrix of a single channel. Substituting r into Eq. (5) gives:

$$246 \quad p = 1 - \exp\left(\frac{1}{2n} \ln \left( \left| I - \frac{rr^T}{1+rr^T} \right| \right)\right). \quad (7)$$

247  
 248 For arbitrary row vectors, a and b, using the matrix property  
 249  $\det(I + a^T b) = 1 + ba^T$ , the new expression for p is:

$$250$$

$$251 \quad p = 1 - \exp\left(\frac{1}{2n} \ln \left( 1 - \frac{r^T r}{1 + r^T r} \right)\right)$$

$$252 \quad = 1 - \exp\left(\frac{1}{2n} \ln \left( \frac{1}{1 + r^T r} \right)\right)$$

$$253 \quad = 1 - \exp\left(-\frac{1}{2n} \ln(1 + r^T r)\right). \quad (8)$$

254 (III) Iteration in a single layer:

255 First, the iteration in a single layer requires the calculation of R.  
 256 Using  $S_a$ ,  $S_\varepsilon$ , K and Eq. (6), R can be calculated. Second, using Eq.  
 257 (8), p of each candidate channel can be calculated. Moreover, the  
 258 channel corresponding to maximum p is the selected channel for this  
 259 iteration. After a channel has been selected, according to Eq. (3) we  
 260 can use  $\hat{S}$  to get  $S_a$  for the next iteration. Finally, channels which

261 are not selected during this iteration are used as the candidate  
262 channels for the next iteration.

263 When selecting  $n$  from  $N$  channels, it is necessary to calculate  
264  $(N-n/2)n \approx Nn$   $p$  values, which is much smaller than  $C_N^n$ . In addition  
265 to high computational efficiency by using this method, another  
266 advantage is that all channels can be recorded in the order in which  
267 they are selected. In the actual application, if  $n'$  channels are  
268 needed, and  $n' < n$ , we will not need to select the channel again,  
269 but record the selected channel only.

270 (IV) Iteration for different altitudes:

271 Because satellite channel sensitivity varies with height, repeating  
272 the iterative process of step (III), selects the optimum channels at  
273 different heights. Assuming there are  $M$  layers in the atmosphere and  
274 selecting  $n$  from  $N$  channels, it is necessary to calculate  $M \cdot (N -$   
275  $n/2)n \approx M \cdot Nn$   $p$  values, a much smaller number than  $M \cdot C_N^n$ . In  
276 this way, different channel sets can be used to evaluate  
277 corresponding height in the retrieved profiles.

278

### 279 **2.3 Statistical inversion method**

280 The inversion methods for the atmospheric temperature profiles can  
281 be summarized in two categories: statistical inversion and physical  
282 inversion. Statistical inversion is essentially a linear regression

283 model which uses a large number of satellite measurements and  
284 atmospheric parameters to match samples and calculate their  
285 correlation coefficient. Then, based on the correlation coefficient, the  
286 required parameters of the independent measurements obtained by  
287 the satellite are retrieved. Because the method does not directly solve  
288 the radiation transfer equation, it has the advantages of fast  
289 calculation speed. In addition, the solution is numerically stable,  
290 which makes it one of the highest precision methods (Chedin et al.,  
291 1985). Therefore, the statistical inversion method will be used for  
292 our channel selection experiment and a regression equation will be  
293 established.

294 According to an empirical orthogonal function, the atmospheric  
295 temperature (or humidity),  $T$ , and the brightness temperature,  $T_b$ , are  
296 expanded as:

297

$$298 \quad T = T^* \cdot A, \quad (9)$$

299

$$300 \quad T_b = T_b^* \cdot A, \quad (10)$$

301

302 where  $T^*$  and  $T_b^*$  are the eigenvectors of the covariance matrix of  
303 temperature (or humidity) and brightness temperature, respectively.

304 A and B stand for the corresponding expansion coefficient vectors of

305 temperature (humidity) and brightness temperature.

306 Using the least squares method and the orthogonal property, the  
307 coefficient conversion matrix,  $V$ , is introduced:

308

$$309 \quad A = V \cdot B, \quad (11)$$

310

$$311 \quad \text{where } V = AB^T(BB^T)^{-1}. \quad (12)$$

312

313 Using the orthogonality, we get:

314

$$315 \quad B = (T_b^*)^T T_b, \quad (13)$$

316

$$317 \quad A = (T^*)^T T. \quad (14)$$

318

319 For convenience, the anomalies of the state vector (atmospheric  
320 temperature),  $T$ , and the observation vector (brightness temperature),  
321  $T_b$ , are taken:

322

$$323 \quad \hat{T} = \bar{T} + \hat{T}' = \bar{T} + GT_b' = \bar{T} + G(T_b - \bar{T}_b), \quad (15)$$

324

325 where  $\hat{T}$  stands for the retrieval atmospheric temperature.  $\bar{T}$  and  
326  $\bar{T}_b$  are the corresponding average values of the elements,

327 respectively.  $\hat{T}'$  and  $T'_b$  represent the corresponding anomalies  
 328 of the elements, respectively.

329 Assuming there are k sets of observations, a sample anomaly  
 330 matrix with k vectors can be constructed:

331

$$332 \quad T' = (t'_1, t'_2, \dots, t'_k), \quad (16)$$

333

$$334 \quad T'_b = (t'_{b1}, t'_{b2}, \dots, t'_{bk}). \quad (17)$$

335

336 Define the inversion error matrix as:

337

$$338 \quad \delta = \bar{T} - \hat{T} = \hat{T}' - T'. \quad (18)$$

339

340 The retrieval error covariance matrix is:

341

$$\begin{aligned}
 342 \quad S_\delta &= \frac{1}{k-n-1} \delta \delta^T \\
 &= \frac{1}{k-n-1} (T' - GT'_b)(T' - GT'_b)^T \\
 343 \quad &= \frac{k-1}{k-n-1} (S_e - G^T S_{xy} - S_{xy} G^T + GS_y G^T), \quad (19)
 \end{aligned}$$

344

345 where

346



$$\begin{aligned}
347 \quad S_e &= \frac{1}{k-1} T' T'{}^T, \\
348 \quad S_y &= \frac{1}{k-1} T_b' T_b'{}^T, \\
349 \quad S_{xy} &= \frac{1}{k-1} T' T_b'{}^T. \tag{20}
\end{aligned}$$

350

351  $S_e$  stands for the sample covariance matrix of  $T$ ,  $S_y$  denotes the  
352 sample covariance matrix of  $T_b$ , and  $S_{xy}$  represents the covariance  
353 matrix of  $T$  and  $T_b$ . The elements on the diagonal of the error  
354 covariance matrix,  $S_\delta$ , represent the retrieval error variance of  $T$ .  
355 The matrix  $G$  that minimizes the overall error variance is the least  
356 squares coefficient matrix of the regression equation (15), which  
357 meets the criteria:

358

$$359 \quad \delta^2 = \text{tr}(S_\delta) = \min. \tag{21}$$

360

361 Taking a derivative of Eq. (21) with respect to  $G$ ,  $\frac{\partial}{\partial G} \text{tr}(S_\delta) = 0 =$   
362  $(-2S_{xy} + 2GS_y)$ , which means that:

363

$$364 \quad G = S_{xy} S_y^{-1}. \tag{22}$$

365

366 Substituting Eq. (22) into Eq. (15) finally gives the least squares  
367 solution as:

368

369 
$$\hat{T} = \bar{T} + S_{xy}S_y^{-1}(T_b - \bar{T}_b). \quad (23)$$

370

371 It should be noted that the least squares solution obtained here  
372 aims to minimize the sum of the error variance for each element in  
373 the atmospheric state vector after retrieval for several times. At  
374 present, statistical multiple regression is widely used in the retrieval  
375 of atmospheric profiles based on atmospheric remote sensing data.  
376 As long as there are enough data,  $S_{xy}$  and  $S_y$  can be determined.

377

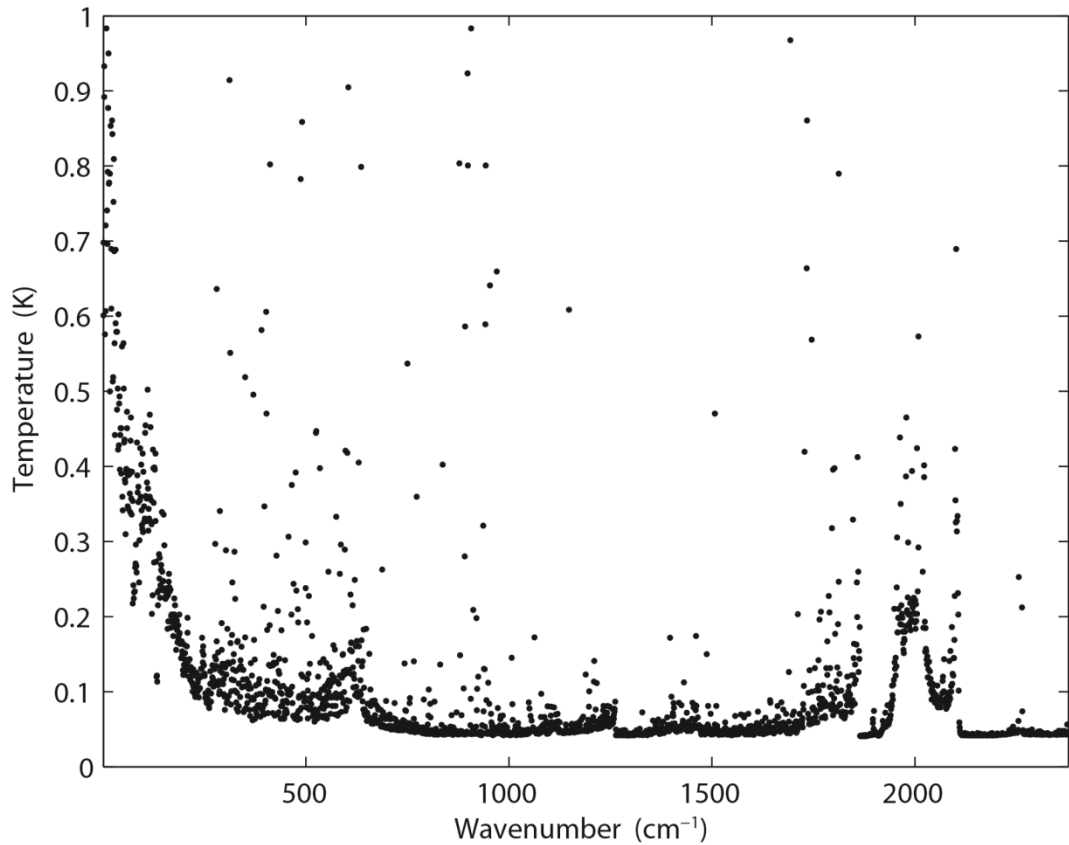
### 378 **3. Channel selection experiment**

#### 379 **3.1 Data and model**

380 The Atmospheric Infrared Sounder (AIRS) is primarily designed to  
381 measure the Earth's atmospheric water vapor and temperature  
382 profiles on a global scale (Aumann et al., 2003; Susskind et al.,  
383 2003). AIRS is a continuously operating cross-track scanning  
384 sounder, consisting of a telescope that feeds an echelle spectrometer.  
385 The AIRS infrared spectrometer acquires 2378 spectral samples at a  
386 resolution  $\lambda/\Delta\lambda$ , ranging from 1086 to 1570, in three bands: 3.74  $\mu\text{m}$   
387 to 4.61  $\mu\text{m}$ , 6.20  $\mu\text{m}$  to 8.22  $\mu\text{m}$ , and 8.8  $\mu\text{m}$  to 15.4  $\mu\text{m}$ . The  
388 footprint size is 13.5 km. The spectral range includes 4.3  $\mu\text{m}$  and  
389 15.5  $\mu\text{m}$  for important temperature observation and  $\text{CO}_2$ , 6.3  $\mu\text{m}$  for

390 water vapor, and 9.6  $\mu\text{m}$  for ozone absorption bands (Menzel et al.,  
391 2018). The root mean square error (RMSE) of the measured  
392 radiation is better than 0.2 K (Susskind et al., 2003). Moreover,  
393 global atmospheric profiles can be detected every day. Due to  
394 radiometer noise and faults, there are currently only 2047 effective  
395 channels. However, compared with previous infrared detectors,  
396 AIRS boasts a significant improvement in both the number of  
397 channels and spectral resolution (Aumann, 1994; Huang et al., 2005;  
398 Li et al., 2005).

399 The root mean square error of an AIRS infrared channel is shown  
400 in Fig. 1. The measurement error is not below 0.2K for all the  
401 instrument channels. There are a few channels with extremely large  
402 measurement errors, which reduce the accuracy of prediction to  
403 some extent. Among them, some extremely large measurement  
404 errors reduce the accuracy of prediction to some extent (Susskind et  
405 al., 2003). At present, more than 300 channels have not been used  
406 because their errors exceed 1 K. If data from these channels were to  
407 be used for retrieval, the accuracy of the retrieval could be reduced.  
408 Therefore, it is necessary to select a group of channels to improve  
409 the calculation efficiency and retrieval quality. In this paper we study  
410 channel selection for temperature profile retrieval by AIRS.



411

412 **Figure 1.** Root mean square error of AIRS infrared channel (black  
 413 spots).

414

415 For the calculation of radiative transfer and the weighting function  
 416 matrix,  $K$ , the RTTOV (Radiative Transfer for TOVS) v12 fast  
 417 radiative transfer model is used. Although initially developed for the  
 418 TOVS (TIROS Operational Vertical Sounder) radiometers, RTTOV  
 419 can now simulate around 90 different satellite sensors measuring in  
 420 the MW (microwave), IR (infrared) and VIS (visible) regions of the  
 421 spectrum (Saunders et al., 2018). The model allows rapid  
 422 simulations (1 ms for 40 channel ATOVS (Advanced TOVS) on a  
 423 desktop PC) of radiances for satellite visible, infrared, or microwave

424 nadir scanning radiometers given atmospheric profiles of  
425 temperature and trace gas concentrations, and cloud and surface  
426 properties. The only mandatory gas included as a variable for  
427 RTTOV v12 is water vapor. Optionally, ozone, carbon dioxide,  
428 nitrous oxide, methane, carbon monoxide, and sulfur dioxide can be  
429 included, with all other constituents assumed to be constant. RTTOV  
430 can accept input profiles on any defined set of pressure levels. The  
431 majority of RTTOV coefficient files are based on the 54 levels (see  
432 Table A1 in Appendix A), in the range from 1050 hPa to 0.01 hPa,  
433 though coefficients for some hyperspectral sounders are also  
434 available on 101 levels.

435 In order to correspond to the selected profiles, the atmosphere is  
436 divided into 137 layers, each of which contains corresponding  
437 atmospheric characteristics, such as temperature, pressure, and the  
438 humidity distribution. Each element in the weighting function matrix  
439 can be written as  $\partial y_i / \partial x_j$ . The subscript  $i$  is used to identify the  
440 satellite channel, and the subscript  $j$  is used to identify the  
441 atmospheric variable. Therefore,  $\partial y_i / \partial x_j$  indicates the variation in  
442 brightness temperature in a given satellite channel, when a given  
443 atmospheric variable in a given layer changes. We are thus able to  
444 establish which layer of the satellite channel is particularly sensitive  
445 to which atmospheric characteristic (temperature, various gas

446 contents) in the vertical atmosphere. The RTTOV\_K (the K mode),  
447 is used to calculate the matrix  $H(X_0)$  (Eq. (1)) for a given  
448 atmospheric profile characteristic.

449

### 450 **3.2 Channel selection comparison experiment and results**

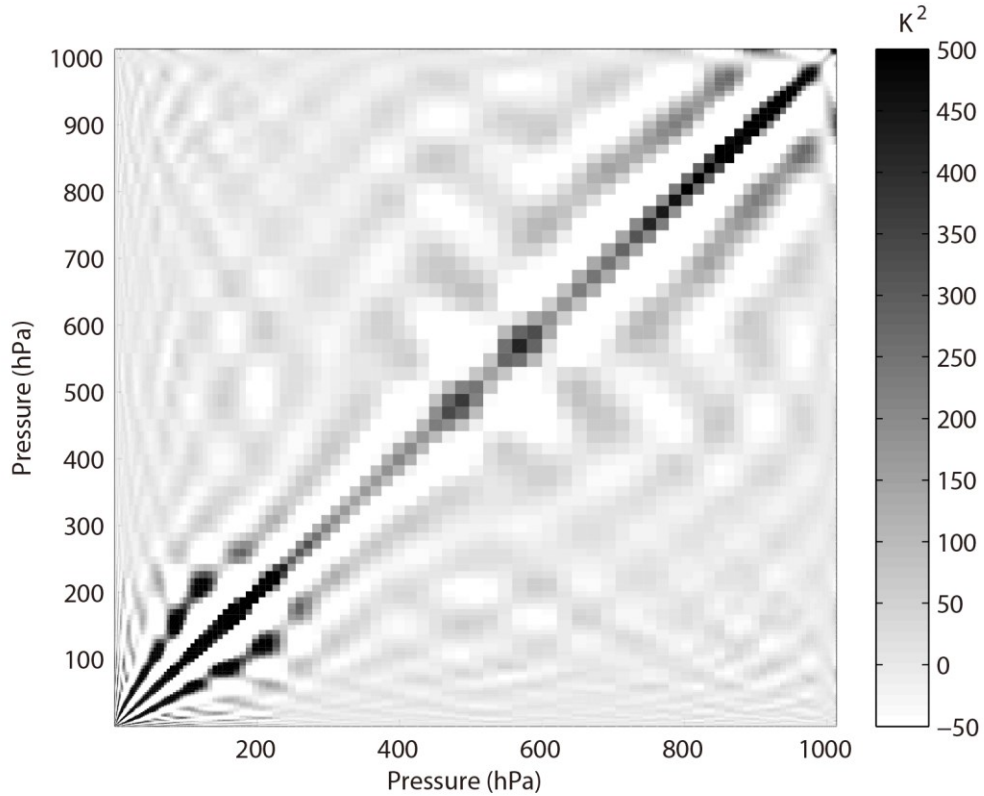
451 In order to verify the effectiveness of the method, three sets of  
452 comparison experiments were conducted. First, 324 channels used  
453 by the EUMETSAT Satellite Application Facility on Numerical  
454 Weather Prediction (NWP SAF) were selected. NCS is short for  
455 NWP channel selection in this paper. NCS were released by the  
456 NWPSAF 1DVar (one-dimensional variational analysis) scheme, in  
457 accordance with the requirements of the NWPSAF (Saunders et al.,  
458 2018). Second, 324 channels were selected using the information  
459 capacity method. This method was adopted by Du et al. (2008)  
460 without the consideration of layering. PCS is short for primary  
461 channel selection in this paper.

462 Third,  $324 \times M$  channels were selected using the information  
463 capacity method for the M layer atmosphere. ICS is short for  
464 improved channel selection in this paper. In order to verify the  
465 retrieval effectiveness after channel selection, statistical inversion  
466 comparison experiments were performed using 5000 temperature  
467 profiles provided by the ECMWF dataset, which will be introduced

468 in Sect. 4.

469 The observation error covariance matrix,  $S_{\varepsilon}$ , in the experiment is  
470 provided by NWP SAF 1Dvar. In general, it can be converted to a  
471 diagonal matrix, the elements of which are the observation error  
472 standard deviation of each hyperspectral detector channel, which is  
473 the square of the root mean square error for each channel. The root  
474 mean square error of the AIRS channels is shown in Fig. 1. The error  
475 covariance matrix of the background,  $S_a$ , is calculated using 5000  
476 samples of the IFS-137 data provided by the ECMWF dataset (The  
477 detailed information will be introduced in Sect. 4). The last access  
478 date is April 26th, 2019 (download address:  
479 <https://www.nwpsaf.eu/site/update-137-level-nwp-profile-dataset/>,  
480 2019). The covariance matrix of temperature is shown in Fig. 2. The  
481 results are consistent with the previous study by Du et al. (2008).

482



483

484 **Figure 2.** Error covariance matrix of temperature (shaded).

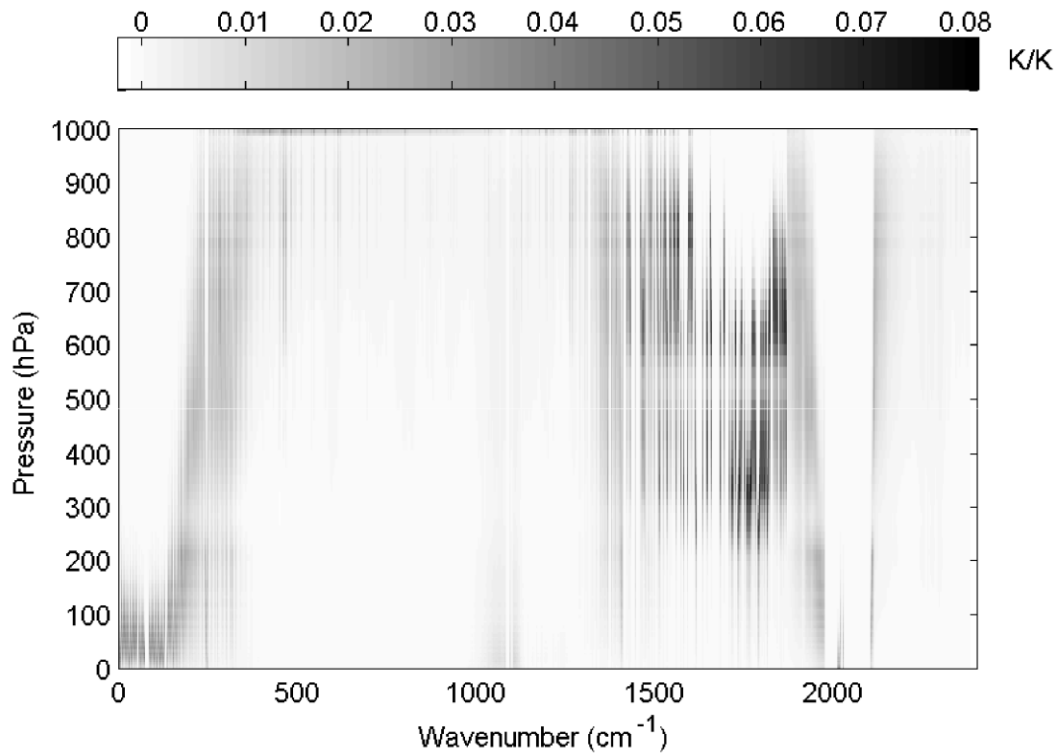
485

486 The reference atmospheric profiles are from the IFS-137 database,  
 487 and the temperature weighting function matrix is calculated using  
 488 the RTTOV\_K mode, as shown in Fig. 3; the results are consistent  
 489 with those of the previous study by Du et al. (2008). For the  
 490 air-based passive atmospheric remote sensing studied in this paper,  
 491 when the same channel detects the atmosphere from different  
 492 observation angles, the value of the weighting function matrix  $K$   
 493 changes due to the limb effect. The goal of this section is focusing  
 494 on the selection methods of selecting channels; therefore the biases  
 495 produced from different observation angles can be ignored.



496

497

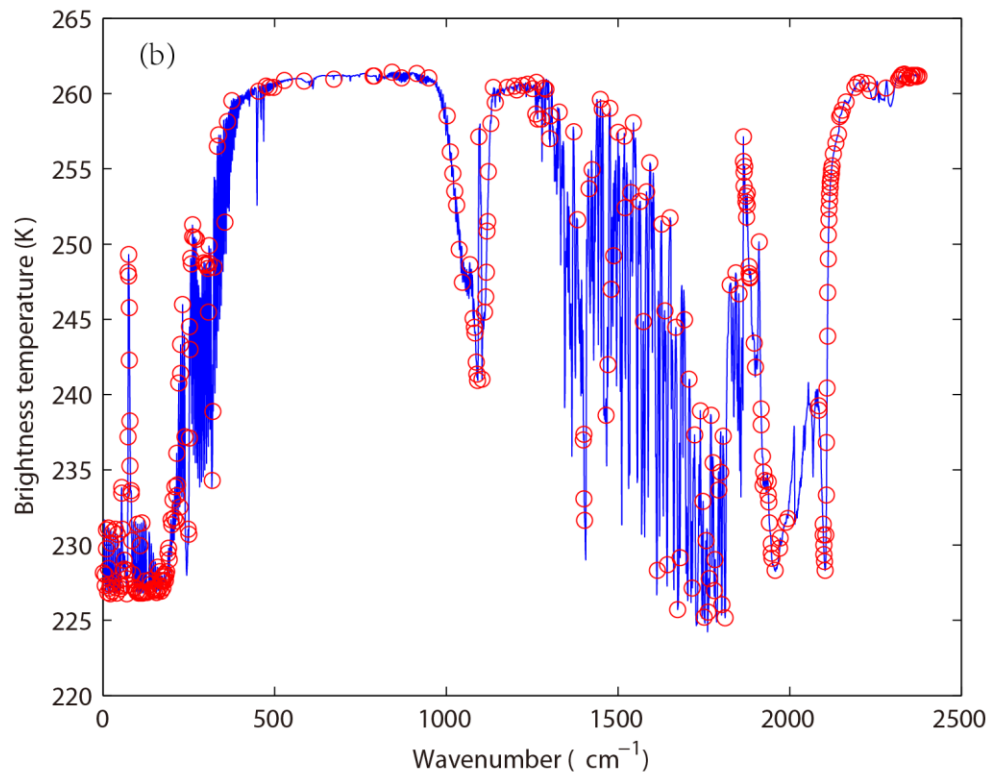
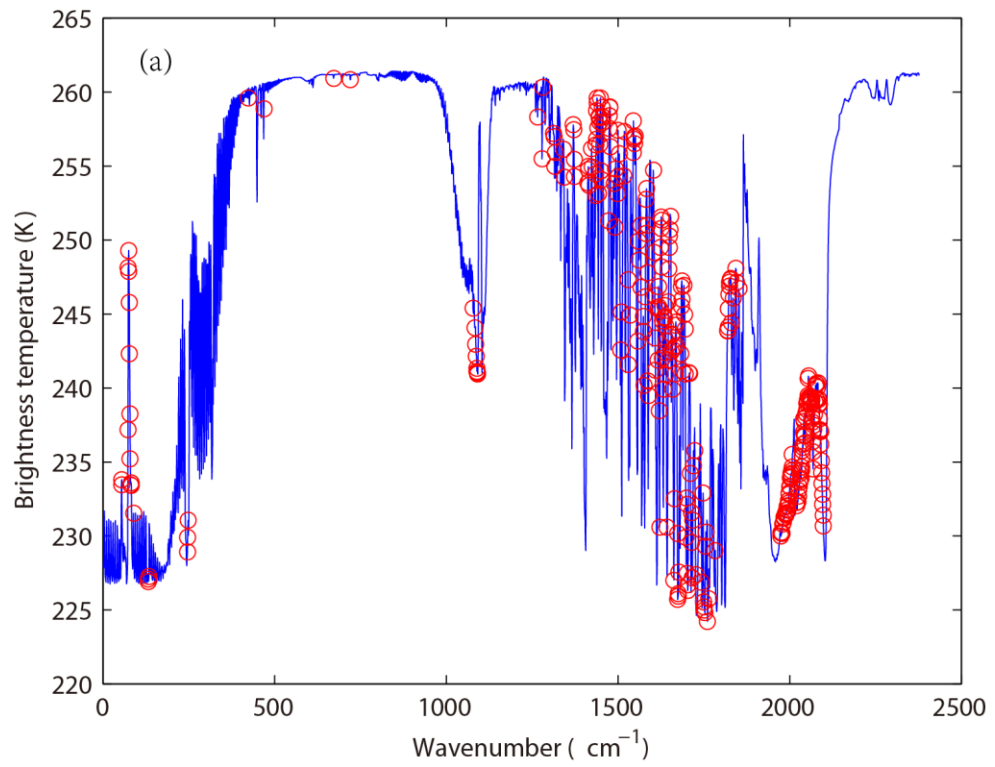


498 **Figure 3.** Temperature weighting function matrix (shaded).

499

500 In order to verify the effectiveness, the distribution of 324  
501 channels, without considering layering, in the AIRS brightness  
502 temperature spectrum is indicated in Fig. 4. The background  
503 brightness temperature is the simulated AIRS observation brightness  
504 temperature, which is from the atmospheric profile in RTTOV put  
505 into the model. Figure 4(a) shows the 324 channels selected by PCS,  
506 while Fig. 4(b) shows the 324 channels selected by NCS.

507



508

509 **Figure 4.** The distribution of different channel selection methods

510 without considering layering in the AIRS brightness temperature

511 spectrum (blue line). (a) 324 channels selected by PCS (red circles).  
512 (b) 324 channels selected by NCS (red circles).

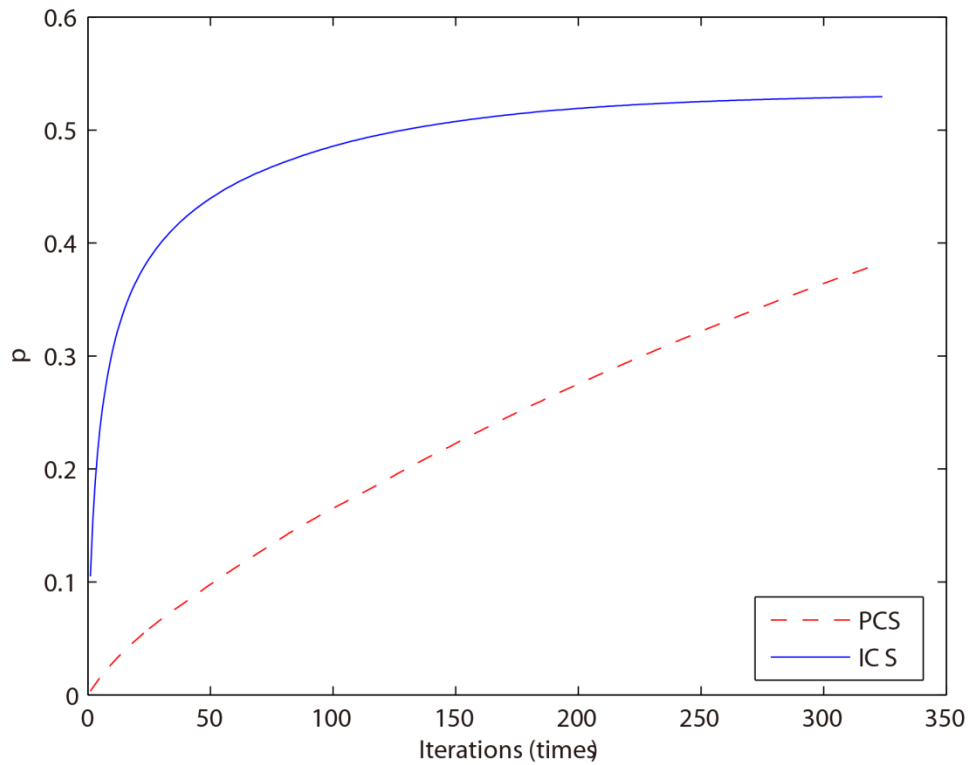
513 Without considering layering, the main differences between the  
514 324 channels selected by PCS and NCS are as follows: (1) Near 10  
515  $\mu\text{m}$  band, fewer channels are selected by PCS because the retrieval  
516 of ground temperature is considered by NCS; (2) Near 9  $\mu\text{m}$  band,  
517 no channels are selected by PCS because the retrieval of  $\text{O}_3$  is not  
518 considered in this paper; (3) As is known, the spectral range from 6  
519  $\mu\text{m}$  to 7  $\mu\text{m}$  corresponds to water vapor absorption bands, but fewer  
520 channels are selected by NCS; (4) Near 5  $\mu\text{m}$  band, it includes 4.2  
521  $\mu\text{m}$  for  $\text{N}_2\text{O}$  and 4.3  $\mu\text{m}$  for  $\text{CO}_2$  absorption bands. As is shown in  
522 Fig. 4, fewer channels are selected by PCS in those bands. PCS is  
523 favorable for atmospheric temperature observation. Because 4.2  $\mu\text{m}$   
524 and 4.3  $\mu\text{m}$  bands are sensitive to high temperature, a better  
525 observation can be obtained for higher temperatures; (5) Near 4  $\mu\text{m}$   
526 band, a small number of channels is selected by NCS, but no  
527 channels are selected by PCS.

528 Above all, the information content considered in this study only  
529 takes the temperature profile retrieval into consideration, so the  
530 channel combination of PCS is inferior to that of NCS for the  
531 retrieval of surface temperature and the  $\text{O}_3$  profile. The advantages  
532 of the channel selection method based on information content in this

533 paper are mainly reflected in: (1) Stratosphere and mesosphere is  
534 less affected by the ground surface, so the retrieval result of PCS is  
535 better than that of NCS. (2) Due to the method selected in this paper  
536 there are more channels at 4.2  $\mu\text{m}$  for  $\text{N}_2\text{O}$  and 4.3  $\mu\text{m}$  for  $\text{CO}_2$   
537 absorption bands; the channel combination of PCS is better than that  
538 of NCS for atmospheric temperature observation at higher  
539 temperature.

540 By comparing channel selection without considering layering,  
541 we note the general advantages and disadvantages of PCS and NCS  
542 for the retrieval of temperature and can improve the channel  
543 selection scheme. First, the retrieval of the temperature profile for  
544 324 channels selected by PCS is obtained. The relationship between  
545 the number of iterations and the ARI is shown in Fig. 5.

546



547

548 **Figure 5.** The relationship between the number of iterations and ARI.

549 Blue line represents the result of ICS. Red dotted line stands for the

550 result of PCS.

551

552 The ARI for PCS tends to be 0.38 and is not convergent, so the

553 PCS method needs to be improved. In this paper, the atmosphere is

554 divided into 137 layers, and based on the information content and

555 iteration, 324 channels are selected for each layer. Then, the

556 temperature profile of each layer can be retrieved based on statistical

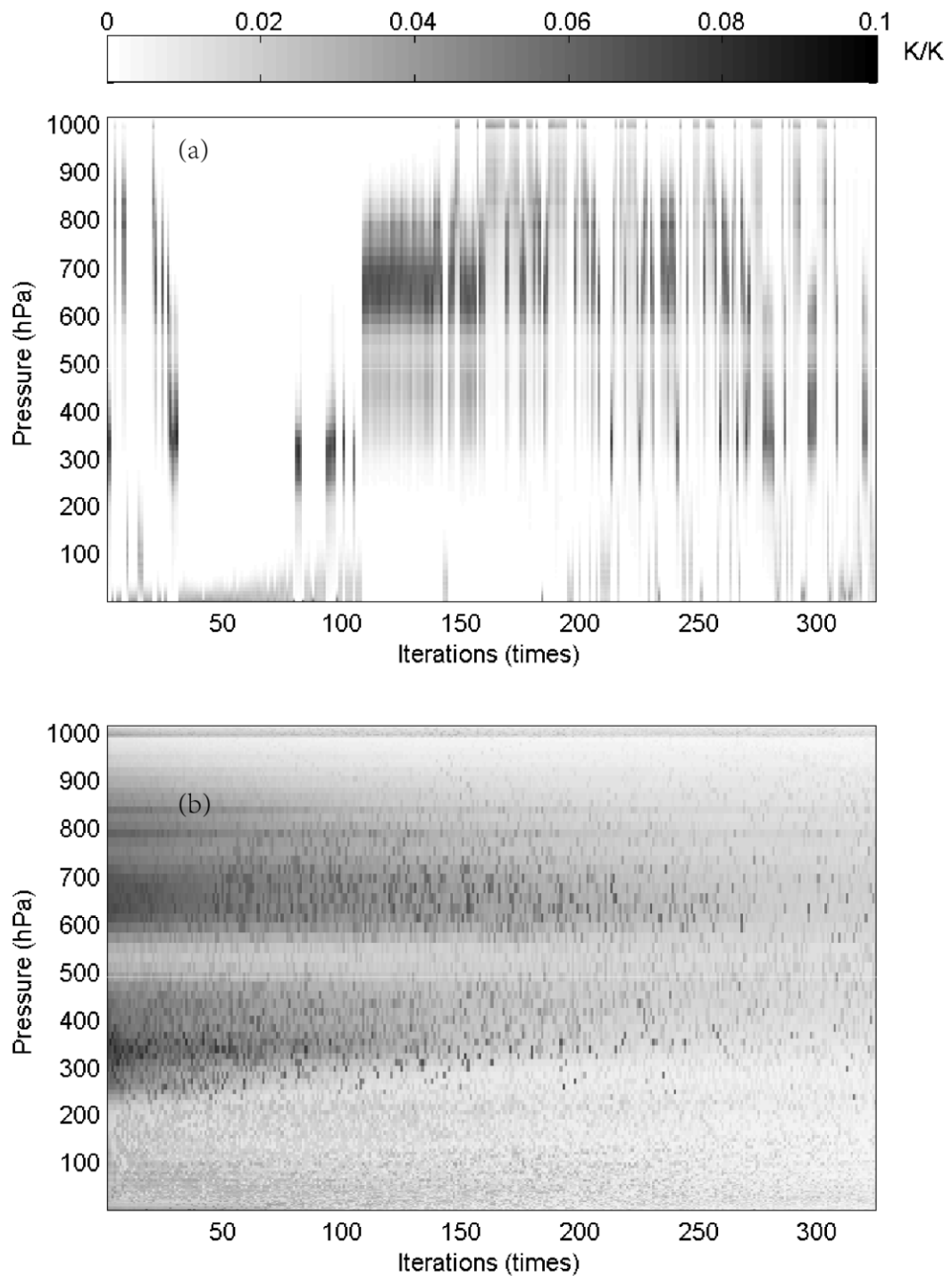
557 inversion (see at Sect. 4). The relationship between the number of

558 iterations and the ARI for ICS is shown in Fig. 5b. When the number

559 of iterations approaches 100, the ARI of ICS tends to be stable, and

560 reaches 0.54. Thus, in terms of the ARI and convergence, the ICS  
561 method is better than that of PCS.

562 Furthermore, because an iterative method is used to select  
563 channels, the order of each selected channel is determined by the  
564 contribution from the ARI. The weighting function matrix of the top  
565 324 selected channels, according to channel order, is shown in Fig.  
566 6.



568 **Figure 6.** The relationship between the number of iterations and the  
 569 weighting function of the top 324 selected channels (shaded). (a)  
 570 ICS. (b) PCS.

571

572 As illustrated in Fig. 6, in the first 100 iterations, the distribution  
573 of the temperature weighting function for PCS is relatively scattered;  
574 it does not reflect continuity between the adjacent layers of the  
575 atmosphere. Besides, the ICS result is better than that of PCS,  
576 showing that: (1) the distribution of the temperature weighting  
577 function is more continuous and reflects the continuity between  
578 adjacent layers of the atmosphere; (2) regardless of the number of  
579 iterations, the maximum value of the weighting function is stable  
580 near 300–400 hPa and 600–700 hPa, without scattering, which is  
581 closer to the situation in real atmosphere.

582

## 583 **4. Statistical multiple regression experiment**

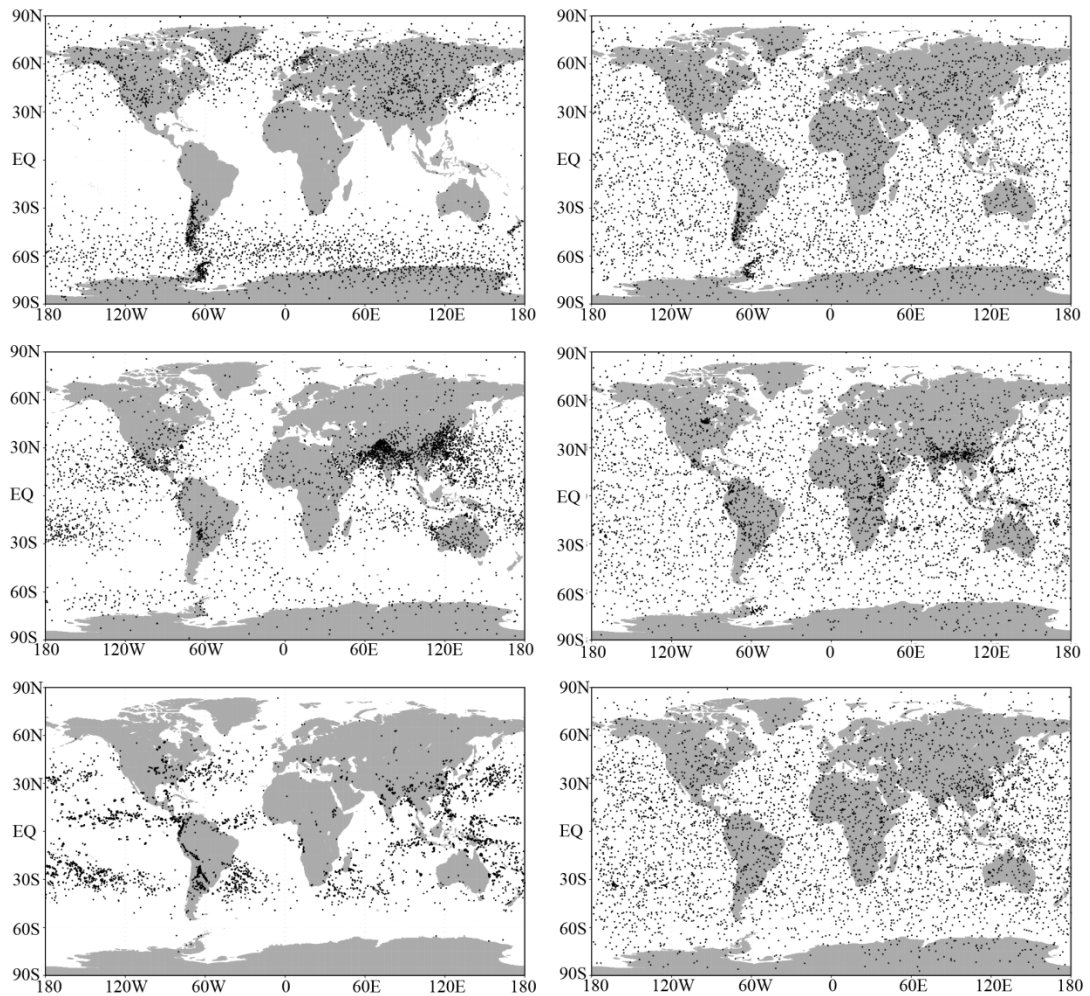
### 584 **4.1 Temperature profile database**

585 A new database including a representative collection of 25,000  
586 atmospheric profiles from the European Centre for Medium-range  
587 Weather Forecasts (ECMWF) was used for the statistical inversion  
588 experiments. The profiles were given in a 137-level vertical grid  
589 extending from the surface up to 0.01 hPa. The database was divided  
590 into five subsets focusing on diverse sampling characteristics such as  
591 temperature, specific humidity, ozone mixing ratio, cloud  
592 condensates, and precipitation. In contrast with earlier releases of the



593 ECMWF diverse profile database, the 137-level database places  
594 greater emphasis on preserving the statistical properties of sampled  
595 distributions produced by the Integrated Forecasting System (IFS)  
596 (Eresmaa and McNally, 2014; Brath et al., 2018). IFS-137 spans the  
597 period from September 1, 2013 to August 31, 2014. There are two  
598 operational analyses each day (at 00z and 12z), and approximately  
599 13 000 atmospheric profiles over the ocean. The pressure levels  
600 adopted for IFS-137 are shown in Table A2 (see Table A2 in  
601 Appendix A).

602 The locations of selected profiles of temperature, specific  
603 humidity, and cloud condensate subsets of the IFS-91 and IFS-137  
604 databases are plotted on the map in Fig. 7. In the IFS-91 database,  
605 the sampling is fully determined by the selection algorithm, which  
606 makes the geographical distributions very inhomogeneous. Selected  
607 profiles represent those regions where gradients of the sampled  
608 variable are the strongest: in the case of temperature, mid- and  
609 high-latitudes dominate, while humidity and cloud condensate  
610 subsets concentrate at low latitudes. However, the IFS-137 database  
611 shows a much more homogeneous spatial distribution in all the  
612 sampling subsets, which is a consequence of the randomized  
613 selection.

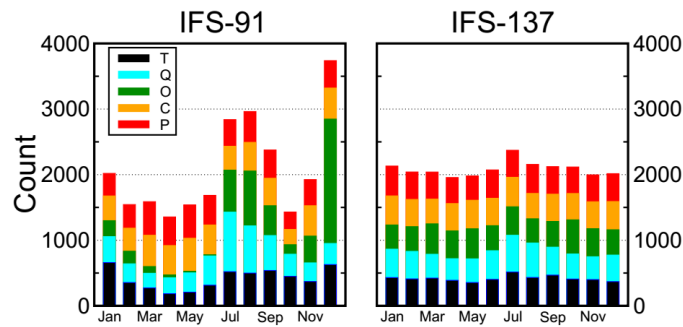


615 **Figure 7.** Locations of selected profiles in the temperature (top),  
 616 specific humidity (middle), and cloud condensate (bottom), sampled  
 617 subsets of the IFS-91 (left) and IFS-137 (right) databases (from  
 618 <https://www.nwpsaf.eu/site/update-137-level-nwp-profile-dataset/> ,  
 619 2019).

620

621 The temporal distribution of the selected profiles is illustrated in Fig.  
 622 8. The coverage of the IFS-137 data set is more homogeneous than

623 the IFS-91 data set. Moreover, the IFS-137 database supports the  
 624 mode with input parameters, such as detection angle, 2 m  
 625 temperature, and cloud information. Therefore, it is feasible to use  
 626 the selected samples in a statistical multiple regression experiment.



627 **Figure 8.** Distribution of profiles within the calendar months in  
 628 IFS-91 (left) and IFS-137 (right) databases. Different subsets are  
 629 shown in different colors. Black parts stand for temperature. Blue  
 630 parts represent specific humidity. Green parts indicate ozone subset.  
 631 Orange parts stand for cloud condensate. Red parts represent  
 632 precipitation. The last access date is April 26th, 2019. (from  
 633 <https://www.nwpsaf.eu/site/update-137-level-nwp-profile-dataset/> ,  
 634 2019).

635

## 636 4.2 Experimental scheme

637 In order to verify the retrieval effectiveness of ICS, 5000  
 638 temperature profiles provided by the IFS-137 were used for  
 639 statistical inversion comparison experiments. The steps are as  
 640 follows:

641 (1) 5000 profiles and their corresponding surface factors,  
642 including surface air pressure, surface temperature, 2 m temperature,  
643 2 m specific humidity, 10 m wind speed are put into the RTTOV  
644 mode. Then, the simulated AIRS spectra are obtained.

645 (2) The retrieval of temperature is carried out in accordance with  
646 Eq. (23). The 5000 profiles are divided into two groups. The first  
647 group of 2500 profiles is used to obtain the regression coefficient,  
648 and the second group of 2500 is used to test the result.

649 (3) Verification of the results. The test is carried out based on the  
650 standard deviation between the retrieval value and the true value.

651

### 652 **4.3 Results and Discussion**

653 For the statistical inversion comparison experiments, the standard  
654 deviation of temperature retrieval is shown in Fig. 9. First, because  
655 PCS does not take channel sensitivity as a function of height into  
656 consideration, the retrieval result of PCS is inferior to that of ICS.  
657 Second, by comparing the results of ICS and NCS we found that  
658 below 100 hPa, since the method used in this paper considers near  
659 ground to be less of an influencing factor, the channel combination  
660 of ICS is slightly inferior to that of NCS, but the difference is small.

661 From 100 hPa to 10 hPa, the retrieval temperature of ICS in this  
662 paper is consistent with that of NCS, slightly better than the channel

663 selected for NCS. From 10 hPa to 0.02 hPa, near the space layer, the  
664 retrieval temperature of ICS is better than that of NCS. In terms of  
665 the standard deviation, the channel combination of ICS is slightly  
666 better than that of PCS from 100 hPa to 10 hPa. From 10 hPa to 0.02  
667 hPa, the standard deviation of ICS is lower than that of NCS at about  
668 1 K, meaning that the retrieval result of ICS is better than that of  
669 NCS.

670 In order to further illustrate the effectiveness of ICS, the mean  
671 improvement value of the ICS and its percentages compared with the  
672 PCS and NCS at different heights are shown in Table 1. Because  
673 PCS does not take channel sensitivity as a function of height into  
674 consideration, the retrieval result of PCS is inferior to that of ICS. In  
675 general, the accuracy of the retrieval temperature of ICS is improved.  
676 Especially, from 100 hPa to 0.01 hPa, the mean value of ICS is  
677 evidently improved by more than 0.5 K which means the accuracy  
678 can be improved by more than 11%. By comparing the results of ICS  
679 and NCS we found that below 100 hPa, since the method used in this  
680 paper considers near ground to be less of an influencing factor, the  
681 channel combination of ICS is slightly inferior to that of NCS, but  
682 the difference is small. From 100 hPa to 0.01 hPa, the mean value of  
683 ICS is improved by more than 0.36 K which means the accuracy can  
684 be improved by more than 9.6%.

685

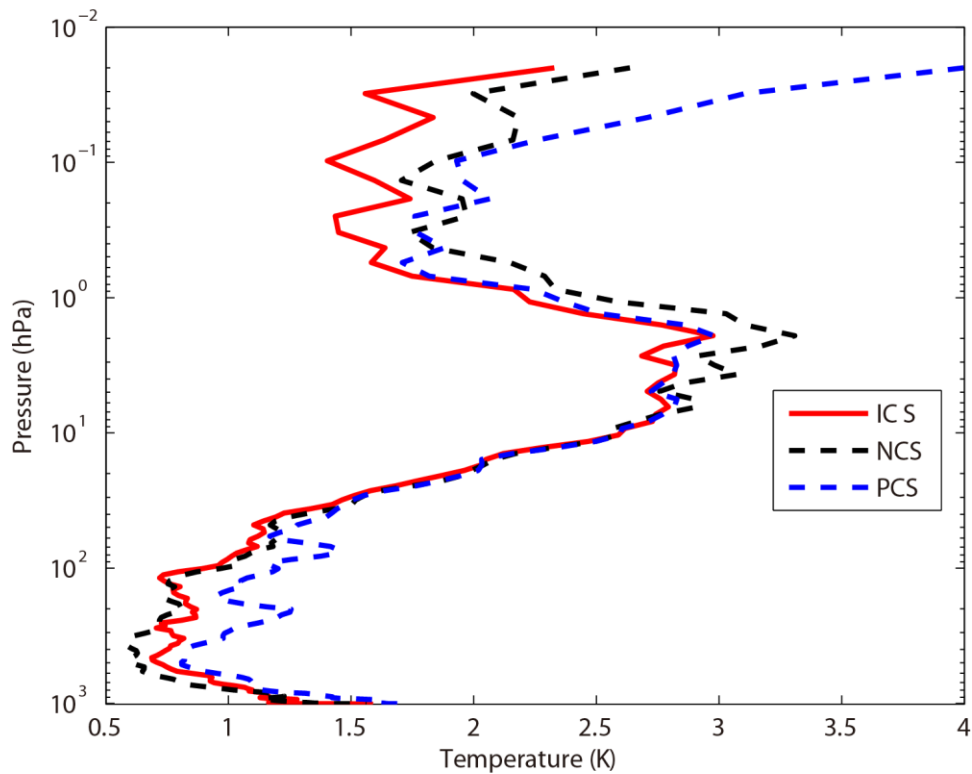
686 **Table 1.** The mean improvement value of the ICS and its  
687 percentages compared with the PCS and NCS at different heights.

Pressure	Improved mean value /Percentage compared with PCS	Improved value /Percentage compared with NCS
hPa	K/%	K/%
surface-100hPa	0.24/10.77%	-0.04/-3.27%
100hPa-10hPa	0.15/5.08%	0.06/2.4%
10hPa-1hPa	0.04/0.64%	0.17/2.99%
1hPa-0.01hPa	0.52/11.92%	0.36/9.57%

688

689 This is because, as shown in Fig. 4: (1) Stratosphere and  
690 mesosphere is less affected by the ground surface, so the retrieval  
691 result of PCS is better than that of NCS. (2) Due to the method  
692 selected in this paper, there are more channels at 4.2  $\mu\text{m}$  for  $\text{N}_2\text{O}$  and  
693 4.3  $\mu\text{m}$  for  $\text{CO}_2$  absorption bands, and the channel combination of  
694 PCS is superior to that of NCS for atmospheric temperature  
695 observation in the high temperature zone. Moreover, ICS takes  
696 channel sensitivity as a function of height into consideration, so its  
697 retrieval result is improved.

698



699

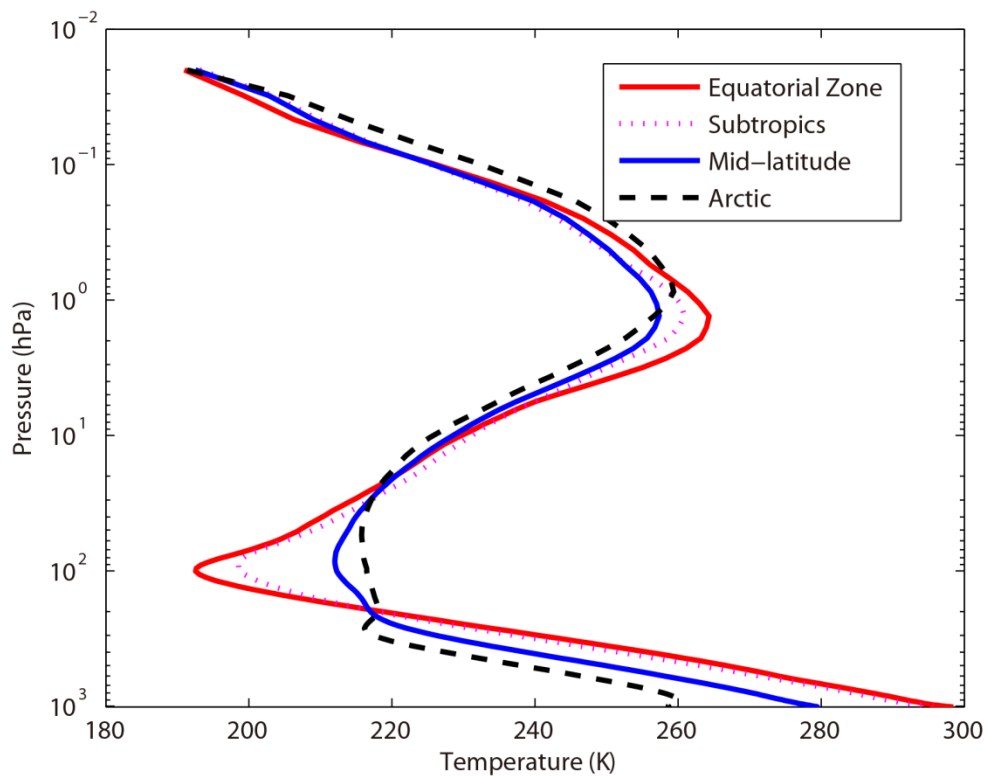
700 **Figure 9.** The temperature profile standard deviation of statistical  
 701 inversion comparison experiments. Red line indicates the result of  
 702 ICS. Black dotted line stands for the result of NCS. Blue dotted line  
 703 represents the result of PCS.

704

705 **5 Statistical inversion comparison experiments in four typical**  
 706 **regions**

707 The accuracy of the retrieval temperature varies from place to place  
 708 and changes with atmospheric conditions. Therefore, in order to  
 709 further compare the inversion accuracy under different atmospheric  
 710 conditions, this paper has divided the atmospheric profile from the  
 711 IFS-137 database introduced in Sect. 4 into four regions: equatorial

712 zone, subtropical region, mid-latitude region and Arctic. The average  
713 temperature profiles in these four regions are shown in Fig. 10. The  
714 retrieval temperature varies from place to place and changes with  
715 atmospheric conditions. In order to further compare the regional  
716 differences of inversion accuracy, the temperature standard  
717 deviations of ICS in four typical regions are compared in Sect. 5.2.  
718



719

720 **Figure 10.** The average temperature profiles in four typical regions.  
721 Red line indicates the equatorial zone. Pink dotted line stands for the  
722 subtropics. Blue dotted line represents the mid-latitude region. Black  
723 dotted line stands for the Arctic.

724



725

## 726 **5.1 Experimental scheme**

727 In order to further illustrate the different accuracy of the retrieval  
728 temperature using our improved channel selection method under  
729 different atmospheric conditions, the profiles in four typical regions  
730 were used for statistical inversion comparison experiments. The  
731 experimental steps are as follows:

732 (1) 2500 profiles in Sect. 4 are used to work out the regression  
733 coefficient.

734 (2) The atmospheric profiles of the four typical regions: equatorial  
735 zone, subtropical region, mid-latitude region and Arctic are used for  
736 statistical inversion comparison experiments and test the result.(3)  
737 Verification of the results. The test is carried out based on the  
738 standard deviation between the retrieval value and the true value.

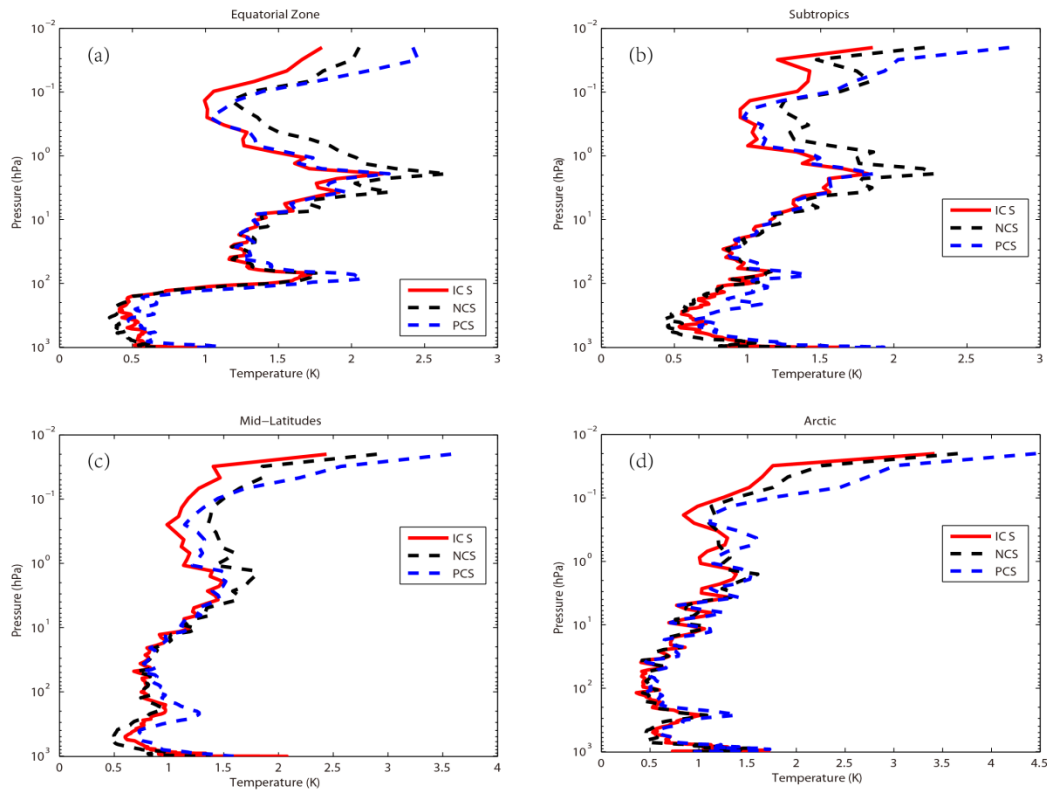
739

## 740 **5.2 Results and Discussion**

741 Using statistical inversion comparison experiments in four typical  
742 regions, the standard deviation of temperature retrieval is shown in  
743 Fig. 11. Generally, the retrieval temperature by ICS is better than  
744 that of NCS and PCS. In particular, above 1 hPa (the stratosphere  
745 and mesosphere), the standard deviation of atmospheric temperature  
746 can be improved by 1 K with PCS and NCS. Thus, ICS shows a

747 great improvement. The results were consistent with Sect. 4.

748



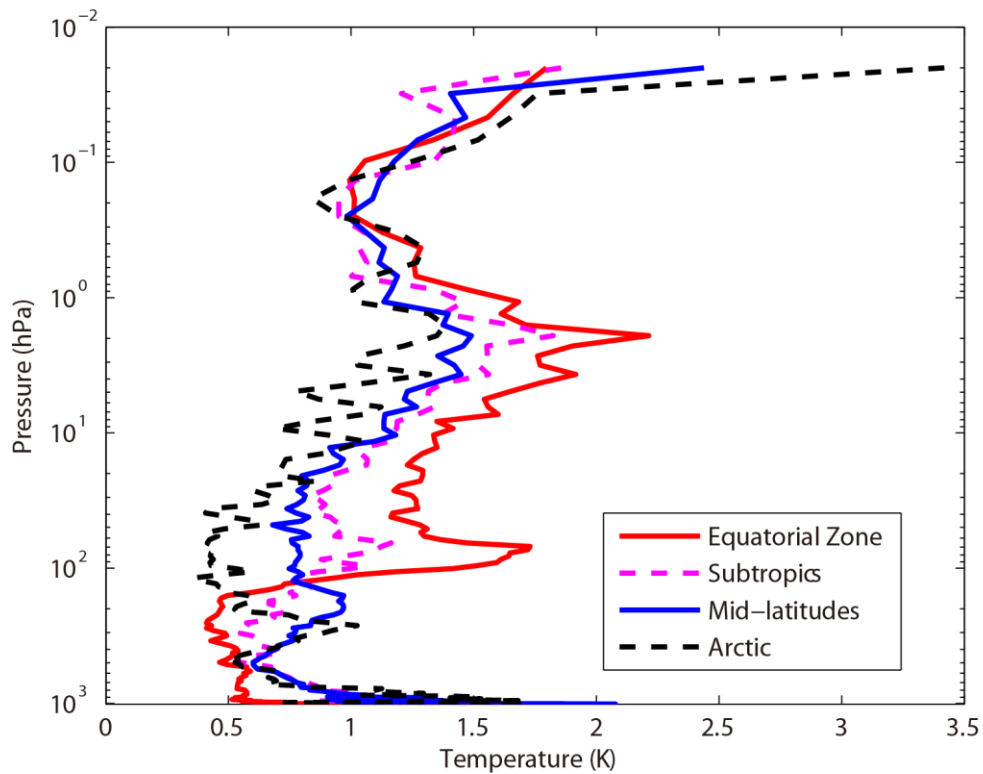
749

750 **Figure 11.** The temperature profile standard deviation of statistical  
751 inversion comparison experiments in four typical regions. Red line  
752 indicates the result of ICS. Black dotted line stands for the result of  
753 NCS. Blue dotted line represents the result of PCS. (a) Equatorial  
754 zone. (b) Subtropics. (c) Mid-latitudes. (d) Arctic.

755

756 In order to further compare the regional differences of inversion  
757 accuracy, the temperature standard deviation of ICS in four typical  
758 regions are compared in Fig. 12.

759



760

761 **Figure 12.** The temperature standard deviation of ICS in four typical  
 762 regions. Red line indicates the result of equatorial zone. Pink dotted  
 763 line represents the result of Subtropics. Blue line represents the  
 764 result of Mid-latitudes. Black dotted line stands for the result of  
 765 Arctic.

766

767 The temperature standard deviations of the ICS in the four typical  
 768 regions are large (Fig. 12). Below 100 hPa, due to the high  
 769 temperature in the equatorial zone, the channel combination of ICS  
 770 is better than that of PCS and NCS for atmospheric temperature  
 771 observation at higher temperature. The standard deviation is 0.5K.  
 772 Due to the method selected in this paper there are more channels at

773 4.2  $\mu\text{m}$  for  $\text{N}_2\text{O}$  and 4.3  $\mu\text{m}$  for  $\text{CO}_2$  absorption bands which has  
774 been previously described in Sect. 3. Near the tropopause, the  
775 standard deviation of the equatorial zone increases sharply. It is also  
776 due to the sharp drops in temperature. However, the standard  
777 deviation of the Arctic is still around 0.5K. From 100hPa to 1hPa,  
778 the standard deviation of ICS is 0.5 K to 2K. With the increase of  
779 latitude, the effectiveness considerably increases. According to Fig.  
780 11, ICS takes channel sensitivity as a function of height into  
781 consideration, so its retrieval result is better.

782 Although the improvements of ICS in the four typical regions are  
783 different, in general, the accuracy of the retrieval temperature of ICS  
784 is improved. Because PCS does not take channel sensitivity as a  
785 function of height into consideration, the retrieval result of PCS is  
786 inferior to that of ICS. In general, the accuracy of the retrieval  
787 temperature of ICS is improved.

788

## 789 **7 Conclusions**

790 In recent years, the atmospheric layer in the altitude range of about  
791 20–100 km has been named “the near space layer” by aeronautical  
792 and astronautical communities. It is between the space-based  
793 satellite platform and the aerospace vehicle platform, which is the  
794 transition zone between aviation and aerospace. Its unique resource

795 has attracted a lot of attention from many countries. Research and  
796 exploration, therefore, on and of the near space layer are of great  
797 importance. A new channel selection scheme and method for  
798 hyperspectral atmospheric infrared sounder AIRS data based on  
799 layering is proposed. The retrieval results of ICS concerning the near  
800 space atmosphere are particularly good. Thus, ICS aims to provide a  
801 new and an effective channel selection method for the study of the  
802 near space atmosphere using the hyperspectral atmospheric infrared  
803 sounder.

804 An improved channel selection method is proposed, based on  
805 information content in this paper. A robust channel selection scheme  
806 and method are proposed, and a series of channel selection  
807 comparison experiments are conducted. The results are as follows:

808 (1) Since ICS takes channel sensitivity as a function of height into  
809 consideration, the ARI of PCS only tends to be 0.38 and is not  
810 convergent. However, as the 100<sup>th</sup> iteration is approached, the ARI of  
811 ICS tends to be stable, reaching 0.54, while the distribution of the  
812 temperature weighting function is more continuous and closer to that  
813 of the actual atmosphere. Thus, in terms of the ARI, convergence,  
814 and the distribution of the temperature weighting function, ICS is  
815 better than PCS.

816 (2) Statistical inversion comparison experiments show that the

817 retrieval temperature of ICS in this paper is consistent with that of  
818 NCS. In particular, from 10 hPa to 0.02 hPa (the stratosphere and  
819 mesosphere), the retrieval temperature of ICS is obviously better  
820 than that of NCS at about 1 K. In general, the accuracy of the  
821 retrieval temperature of ICS is improved. Especially, from 100 hPa  
822 to 0.01 hPa, the accuracy of ICS can be improved by more than 11%.  
823 The reason is that stratosphere and mesosphere are less affected by  
824 the ground surface, so the retrieval result of ICS is better than that of  
825 NCS. Additionally, due to the method selected in this paper there are  
826 more channels at 4.2  $\mu\text{m}$  for the  $\text{N}_2\text{O}$  and at 4.3  $\mu\text{m}$  for the  $\text{CO}_2$   
827 absorption bands; the channel combination of ICS is better than that  
828 of NCS for atmospheric temperature observation at higher  
829 temperature.

830 (3) Statistical inversion comparison experiments in four typical  
831 regions indicate that ICS in this paper is significantly better than  
832 NCS and PCS in different regions and shows latitudinal variations,  
833 which shows potential for future applications.

834

835 *Data availability.* The data used in this paper are available from the  
836 corresponding author upon request.

837

838 *Appendices*

839 Appendix A

840 **Table A1.** Pressure levels adopted for RTTOV v12 54 pressure level  
 841 coefficients and profile limits within which the transmittance  
 842 calculations are valid. Note that the gas units here are ppmv.  
 843 (From <https://www.nwpsaf.eu/site/software/rttov/>, RTTOV Users  
 844 guide, 2019).

Level	Pressure	Tmax	Tmin	Qmax	Qmin	Q <sub>2</sub> max	Q <sub>2</sub> min	Q <sub>2</sub> Ref
Number	hPa	K	K	ppmv*	ppmv*	ppmv*	ppmv*	ppmv*
1	0.01	245.95	143.66	5.24	0.91	1.404	0.014	0.296
2	0.01	252.13	154.19	6.03	1.08	1.410	0.069	0.321
3	0.03	263.71	168.42	7.42	1.35	1.496	0.108	0.361
4	0.03	280.12	180.18	8.10	1.58	1.670	0.171	0.527
5	0.13	299.05	194.48	8.44	1.80	2.064	0.228	0.769
6	0.23	318.64	206.21	8.59	1.99	2.365	0.355	1.074
7	0.41	336.24	205.66	8.58	2.49	2.718	0.553	1.471
8	0.67	342.08	197.17	8.34	3.01	3.565	0.731	1.991
9	1.08	340.84	189.50	8.07	3.30	5.333	0.716	2.787
10	1.67	334.68	179.27	7.89	3.20	7.314	0.643	3.756
11	2.50	322.5	176.27	7.75	2.92	9.191	0.504	4.864
12	3.65	312.51	175.04	7.69	2.83	10.447	0.745	5.953
13	5.19	303.89	173.07	7.58	2.70	12.336	1.586	6.763
14	7.22	295.48	168.38	7.53	2.54	12.936	1.879	7.109
15	9.84	293.33	166.30	7.36	2.46	12.744	1.322	7.060
16	13.17	287.05	163.47	7.20	2.42	11.960	0.719	6.574
17	17.33	283.36	161.49	6.96	2.20	11.105	0.428	5.687
18	22.46	280.93	161.47	6.75	1.71	9.796	0.278	4.705
19	28.69	282.67	162.09	6.46	1.52	8.736	0.164	3.870
20	36.17	279.93	162.49	6.14	1.31	7.374	0.107	3.111

21	45.04	27315	164.66	5.90	1.36	6.799	0.055	2.478
22	55.44	265.93	166.19	6.21	1.30	5.710	0.048	1.907
23	67.51	264.7	167.42	9.17	1.16	4.786	0.043	1.440
24	81.37	261.95	159.98	17.89	0.36	4.390	0.038	1.020
25	97.15	262.43	163.95	20.30	0.01	3.619	0.016	0.733
26	114.94	259.57	168.59	33.56	0.01	2.977	0.016	0.604
27	134.83	259.26	169.71	102.24	0.01	2.665	0.016	0.489
28	156.88	260.13	169.42	285.00	0.01	2.351	0.013	0.388
29	181.14	262.27	17063	714.60	0.01	1.973	0.010	0.284
30	207.61	264.45	174.11	1464.00	0.01	1.481	0.013	0.196
31	236.28	270.09	177.12	2475.60	0.01	1.075	0.016	0.145
32	267.10	277.93	181.98	4381.20	0.01	0.774	0.015	0.110
33	300.00	285.18	184.76	6631.20	0.01	0.628	0.015	0.086
34	334.86	293.68	187.69	9450.00	1.29	0.550	0.016	0.073
35	371.55	300.12	190.34	12432.00	1.52	0.447	0.015	0.063
36	409.89	302.63	194.40	15468.00	2.12	0.361	0.015	0.057
37	449.67	304.43	198.46	18564.00	2.36	0.284	0.015	0.054
38	490.&5	307.2	201.53	21684.00	2.91	0.247	0.015	0.052
39	532.56	31217	202.74	24696.00	3.67	0.199	0.015	0.050
40	572.15	31556	201.61	27480.00	3.81	0.191	0.012	0.050
41	618.07	318.26	189.95	30288.00	6.82	0.171	0.010	0.049
42	661.00	321.71	189.95	32796.00	6.07	0.128	0.009	0.048
43	703.59	327.95	189.95	55328.00	6.73	0.124	0.009	0.047
44	745.48	333.77	189.95	37692.00	8.71	0.117	0.009	0.046
45	786.33	336.46	189.95	39984.00	8.26	0.115	0.008	0.045
46	825.75	338.54	189.95	42192.00	7.87	0.113	0.008	0.043
47	863.40	342.55	189.95	44220.00	7.53	0.111	0.007	0.041
48	898.93	346.23	189.95	46272.00	7.23	0.108	0.006	0.040
49	931.99	34924	189.95	47736.00	6.97	0.102	0.006	0.038
50	962.26	349.92	189.95	51264.00	6.75	0.099	0.006	0.034



51	989.45	350.09	189.95	49716.00	6.57	0.099	0.006	0.030
52	1013.29	360.09	189.95	47208.00	6.41	0.094	0.006	0.028
53	1033.54	350.09	189.95	47806.00	6.29	0.094	0.006	0.027
54	1050.00	350.09	189.95	47640.00	6.19	0.094	0.006	0.027

845

846 **Table A2.** Pressure levels adopted for IFS-137 137 pressure levels

847 (in hPa).

Level number	pressure hPa	Level number	pressure hPa	Level number	pressure hPa	Level number	pressure hPa	Level number	pressure hPa
1	0.02	31	12.8561	61	106.4153	91	424.019	121	934.7666
2	0.031	32	14.2377	62	112.0681	92	441.5395	122	943.1399
3	0.0467	33	15.7162	63	117.9714	93	459.6321	123	950.9082
4	0.0683	34	17.2945	64	124.1337	94	478.3096	124	958.1037
5	0.0975	35	18.9752	65	130.5637	95	497.5845	125	964.7584
6	0.1361	36	20.761	66	137.2703	96	517.4198	126	970.9046
7	0.1861	37	22.6543	67	144.2624	97	537.7195	127	976.5737
8	0.2499	38	24.6577	68	151.5493	98	558.343	128	981.7968
9	0.3299	39	26.7735	69	159.1403	99	579.1926	129	986.6036
10	0.4288	40	29.0039	70	167.045	100	600.1668	130	991.023
11	0.5496	41	31.3512	71	175.2731	101	621.1624	131	995.0824
12	0.6952	42	33.8174	72	183.8344	102	642.0764	132	998.8081
13	0.869	43	36.4047	73	192.7389	103	662.8084	133	1002.225
14	1.0742	44	39.1149	74	201.9969	104	683.262	134	1005.356
15	1.3143	45	41.9493	75	211.6186	105	703.3467	135	1008.224
16	1.5928	46	44.9082	76	221.6146	106	722.9795	136	1010.849
17	1.9134	47	47.9915	77	231.9954	107	742.0855	137	1013.25
18	2.2797	48	51.199	78	242.7719	108	760.5996		
19	2.6954	49	54.5299	79	253.9549	109	778.4661		
20	3.1642	50	57.9834	80	265.5556	110	795.6396		
21	3.6898	51	61.5607	81	277.5852	111	812.0847		
22	4.2759	52	65.2695	82	290.0548	112	827.7756		
23	4.9262	53	69.1187	83	302.9762	113	842.6959		
24	5.6441	54	73.1187	84	316.3607	114	856.8376		
25	6.4334	55	77.281	85	330.2202	115	870.2004		
26	7.2974	56	81.6182	86	344.5663	116	882.791		
27	8.2397	57	86.145	87	359.4111	117	894.6222		
28	9.2634	58	90.8774	88	374.7666	118	905.7116		
29	10.372	59	95.828	89	390.645	119	916.0815		

848 *Author contributions.* ZS contributed the central idea. SC, ZS and  
849 HD conceived the method, developed the retrieval algorithm and  
850 discussed the results. SC analyzed the data, prepared the figures and  
851 wrote the paper. WG contributed to refining the ideas, carrying out  
852 additional analyses. All co-authors reviewed the paper.

853

854 *Competing interests.* The authors declare that they have no conflict  
855 of interest.

856

857 *Acknowledgements.* The study was supported by the National Key  
858 Research Program of China: Development of high-resolution data  
859 assimilation technology and atmospheric reanalysis data set in East  
860 Asia (Research on remote sensing telemetry data assimilation  
861 technology, Grant no. 2017YFC1501802). The study was also  
862 supported by the National Natural Science Foundation of China  
863 (Grant no. 41875045) and Hunan Provincial Innovation Foundation  
864 for Postgraduate (Grant no. CX2018B033 and no. CX2018B034).

865

## 866 **References**

867 Aires, F., Schmitt, M., Chedin, A., and Scott, N.: The “weighting  
868 smoothing” regularization of MLP for Jacobian stabilization,

869 IEEE. T. Neural. Networks., 10, 1502-1510,  
870 <https://doi.org/10.1109/72.809096>, 1999.

871 Aires, F., Chédin, Alain., Scott, N. A., and Rossow, W. B.: A  
872 regularized neural net approach for retrieval of atmospheric and  
873 surface temperatures with the IASI instrument, J. Appl. Meteorol.,  
874 41,144-159,  
875 [https://doi.org/10.1175/1520-0450\(2002\)041<0144:ARNNAF>2.0](https://doi.org/10.1175/1520-0450(2002)041<0144:ARNNAF>2.0)  
876 .CO;2, 2002.

877 Aumann, H. H.: Atmospheric infrared sounder on the earth  
878 observing system, Optl. Engr., 33, 776-784,  
879 <https://doi.org/10.1117/12.159325>, 1994.

880 Aumann, H. H., Chahine, M. T., Gautier, C., and Goldberg, M.:  
881 AIRS/AMSU/HSB on the Aqua mission: design, science objective,  
882 data products, and processing systems, IEEE. Trans. GRS.,  
883 41,253-264, <http://dx.doi.org/10.1109/TGRS.2002.808356>, 2003.

884 Brath, M., Fox, S., Eriksson, P., Harlow, R. C., Burgdorf, M., and  
885 Buehler, S. A.: Retrieval of an ice water path over the ocean from  
886 ISMAR and MARSS millimeter and submillimeter brightness  
887 temperatures, Atmos. Meas. Tech., 11, 611–632,  
888 <https://doi.org/10.5194/amt-11-611-2018>, 2018.

889 Chahine, M. I.: A general relaxation method for inverse solution of  
890 the full radiative transfer equation, J. Atmos. Sci., 29, 741-747,

891 [https://doi.org/10.1175/1520-0469\(1972\)029<0741:AGRMFI>2.0](https://doi.org/10.1175/1520-0469(1972)029<0741:AGRMFI>2.0)  
892 CO;2, 1972.

893 Chang, K. W, L'Ecuyer, T. S., Kahn, B. H., and Natraj, V.:  
894 Information content of visible and midinfrared radiances for  
895 retrieving tropical ice cloud properties, *J. Geophys. Res.*, 122,  
896 <https://doi.org/10.1002/2016JD026357>, 2017.

897 Chedin, A., Scott, N. A., Wahiche, C., and Moulinier, P.: The  
898 improved initialization inversion method: a high resolution  
899 physical method for temperature retrievals from satellites of the  
900 tiros-n series, *J. Appl. Meteor.*, 24, 128-143,  
901 [https://doi.org/10.1175/1520-0450\(1985\)024<0128:TIHIMA>2.0.C](https://doi.org/10.1175/1520-0450(1985)024<0128:TIHIMA>2.0.C)  
902 O;2, 1985.

903 Cyril, C., Alain, C., and Scott, N. A.: Airs channel selection for CO<sub>2</sub>  
904 and other trace-gas retrievals, *Q. J. Roy. Meteor. Soc.*, 129,  
905 2719-2740, <https://doi.org/10.1256/qj.02.180>, 2003.

906 Du, H. D., Huang, S. X., and Shi, H. Q.: Method and experiment of  
907 channel selection for high spectral resolution data, *Acta. Physica.*  
908 *Sinica.*, 57, 7685-7692, 2008 .

909 Dudhia, A., Jay, V. L., and Rodgers, C. D.: Microwindow selection  
910 for high-spectral-resolution sounders, *Appl. Opt.* 41, 3665-3673,  
911 <https://doi.org/10.1364/AO.41.003665>, 2002.

912 Eresmaa, R. and McNally, A. P.: Diverse profile datasets from the

913 ECMWF 137-level short-range forecasts, Tech. rep., ECMWF,  
914 2014.

915 Eyre, J. R., Andersson E., and McNally, A. P.: Direct use of  
916 satellite sounding radiances in numerical weather prediction, High  
917 Spectral Resolution Infrared Remote Sensing for Earth's Weather  
918 and Climate Studies, Springer, Berlin, Heidelberg,  
919 [https://doi.org/10.1007/978-3-642-84599-4\\_25](https://doi.org/10.1007/978-3-642-84599-4_25), 1993.

920 Fang, Z. Y.: The evolution of meteorological satellites and the  
921 insight from it, *Adv. Meteorol. Sci. Technol.*, 4, 27-34,  
922 <https://doi.org/10.3969/j.issn.2095-1973.2014.06.003>, 2014.

923 Gong, J., Wu, D. L., and Eckermann, S. D.: Gravity wave variances  
924 and propagation derived from AIRS radiances, *Atmos. Chem.*  
925 *Phys.*, 11, 11691-11738,  
926 <https://doi.org/10.5194/acp-12-1701-2012>, 2011.

927 He, M. Y., Du, H. D., Long, Z. Y., and Huang, S. X.: Selection of  
928 regularization parameters using an atmospheric retrievable index  
929 in a retrieval of atmospheric profile, *Acta. Physica Sinica.*, 61,  
930 024205-160, 2012.

931 Hoffmann, L. and Alexander, M. J.: Retrieval of stratospheric  
932 temperatures from atmospheric infrared sounder radiance  
933 measurements for gravity wave studies, *J. Geophys. Res. Atm.*,  
934 114, <https://doi.org/10.1029/2008JD011241>, 2009.

935 Huang, H. L., Li, J., Baggett, K., Smith, W. L., and Guan, L.:  
936 Evaluation of cloud-cleared radiances for numerical weather  
937 prediction and cloud-contaminated sounding applications,  
938 Atmospheric and Environmental Remote Sensing Data Processing  
939 and Utilization: Numerical Atmospheric Prediction and  
940 Environmental Monitoring, I. S. O. Photonics.,  
941 <https://doi.org/10.1117/12.613027>, 2005.

942 Kuai, L., Natraj, V., Shia, R. L., Miller, C., and Yung, Y. L.: Channel  
943 selection using information content analysis: a case study of CO<sub>2</sub>  
944 retrieval from near infrared measurements. J. Q. S. Radiative.  
945 Transfer., 111, 1296-1304,  
946 <https://doi.org/10.1016/j.jqsrt.2010.02.011>, 2010.

947 Li, J., Wolf, W. W., Menzel, W. P., Paul, Menzel. W., Zhang, W. J.,  
948 Huang, H. L., and Achtor, T. H.: Global soundings of the  
949 atmosphere from ATOVS measurements: the algorithm and  
950 validation, J. Appl. Meteor., 39, 1248-1268,  
951 [https://doi.org/10.1175/1520-0450\(2000\)039<1248:GSOTAF>2.0](https://doi.org/10.1175/1520-0450(2000)039<1248:GSOTAF>2.0).  
952 CO;2, 2000.

953 Li, J., Liu, C. Y., Huang, H. L., Schmit, T. J., Wu, X., Menzel, W. P.,  
954 and Gurka, J. J.: Optimal cloud-clearing for AIRS radiances using  
955 MODIS, IEEE. Trans. GRS. , 43, 1266-1278, [http://dx.doi.org/](http://dx.doi.org/10.1109/tgrs.2005.847795)  
956 [10.1109/tgrs.2005.847795](http://dx.doi.org/10.1109/tgrs.2005.847795), 2005.

957 Liu, Z. Q.: A regional ATOVS radiance-bias correction scheme for  
958 radiance assimilation, *Acta. Meteorologica. Sinica.*, 65, 113-123,  
959 2007.

960 Lupu, C., Gauthier, P., and Laroche, Stéphane.: Assessment of the  
961 impact of observations on analyses derived from observing system  
962 experiments, *Mon. Weather. Rev.*, 140, 245-257,  
963 <https://doi.org/10.1175/MWR-D-10-05010.1>, 2012.

964 Menke, W.: *Geophysical Data Analysis: Discrete Inverse Theory*,  
965 Acad. Press., Columbia University, New York,  
966 <https://doi.org/10.1016/B978-0-12-397160-9.00019-9>, 1984.

967 Menzel, W. P., Schmit, T. J., Zhang, P. and Li, J.: Satellite-based  
968 atmospheric infrared sounder development and applications, *Bull.*  
969 *Amer. Meteor. Soc.*, 99, 583–603,  
970 <https://doi.org/10.1175/BAMS-D-16-0293.1>, 2018.

971 Prunet, P., Thépaut J. N., and Cass, V.: The information content of  
972 clear sky IASI radiances and their potential for numerical weather  
973 prediction, *Q. J. Roy. Meteor. Soc.*, 124, 211-241,  
974 <https://doi.org/10.1002/qj.49712454510>, 2010.

975 Xu, Q.: Measuring information content from observations for data  
976 assimilation: relative entropy versus shannon entropy difference,  
977 *Tellus. A.*, 59, 198-209,  
978 <https://doi.org/10.1111/j.1600-0870.2006.00222.x>, 2007.

979 Rabier, F., Fourrié, N., and Chafâi, D.: Channel selection methods  
980 for infrared atmospheric sounding interferometer radiances, Q. J.  
981 Roy. Meteor. Soc., 128, 1011-1027,  
982 <https://doi.org/10.1256/0035900021643638>, 2010.

983 Richardson, M. and Stephens, G. L.: Information content of oco-2  
984 oxygen a-band channels for retrieving marine liquid cloud  
985 properties, Atmospheric Measurement Techniques, 11, 1-19,  
986 <https://doi.org/10.5194/amt-11-1515-2018>, 2018.

987 Rodgers, C. D.: Information content and optimisation of high  
988 spectral resolution remote measurements, Adv. Spa. Research, 21,  
989 136-147, [https://doi.org/10.1016/S0273-1177\(97\)00915-0](https://doi.org/10.1016/S0273-1177(97)00915-0), 1996.

990 Rodgers, C. D.: Inverse Methods for Atmospheric Sounding, Inverse  
991 methods for atmospheric sounding, World Scientific,  
992 <https://doi.org/10.1142/3171>, 2000.

993 Saunders, R., Hocking, J., Turner, E., Rayer, P., Rundle, D., Brunel,  
994 P., Vidot, J., Roquet, P., Matricardi, M., Geer, A., Bormann, N.,  
995 and Lupu, C.: An update on the RTTOV fast radiative transfer  
996 model (currently at version 12), Geosci. Model Dev., 11,  
997 2717-2737, <https://doi.org/10.5194/gmd-11-2717-2018>, 2018.

998 Susskind, J., Barnett, C. D. and Blaisdell, J. M.: Retrieval of  
999 atmospheric and surface parameters from AIRS/AMSU/HSB data  
1000 in the presence of clouds, IEEE Trans. Geosci. Remote Sensing,



1001 41, 390-409, <https://doi.org/10.1109/TGRS.2002.808236>, 2003.

1002 Smith, W. L., Woolf, H. M., and Revercomb, H. E.: Linear  
1003 simultaneous solution for temperature and absorbing constituent  
1004 profiles from radiance spectra, *Appl. Optics.*, 30, 1117,  
1005 <https://doi.org/10.1364/AO.30.001117>, 1991.

1006 Wakita, H., Tokura, Y., Furukawa, F., and Takigawa, M.: Study of  
1007 the information content contained in remote sensing data of  
1008 atmosphere, *Acta. Physica. Sinica.*, 59, 683-691, 2010.

1009 Wang, G., Lu, Q. F., Zhang, J. W., and Wang, H. Y.,.: Study on  
1010 method and experiment of hyper-spectral atmospheric infrared  
1011 sounder channel selection, *Remote Sensing Technology and  
1012 Application.*, 29, 795-802 , 2014.

1013 Zhang, J. W., Wang, G., Zhang, H., Huang J., Chen J., and Wu, L. L.:  
1014 Experiment on hyper-spectral atmospheric infrared sounder  
1015 channel selection based on the cumulative effect coefficient of  
1016 principal component, *Journal of Nanjing Institute of meteorology*,  
1017 1, 36-42, <http://dx.doi.org/10.3969/j.issn.1674-7097.2011.01.005>,  
1018 2011.